Versatile approach to synthesis of 2-D hexagonal ultra-large-pore periodic mesoporous organosilicas†

Manik Mandal[ab] and Michal Kruk*[ab]

Received 22nd April 2010, Accepted 20th June 2010
DOI: 10.1039/c0jm01170c

Periodic mesoporous organosilicas (PMOs) with methylene (–CH_2–), ethylene (–CH_2CH_2–), ethenylene (–CH=CH–) and phenylene (–C_6H_4–) framework groups were synthesized with 2-dimensional hexagonal structures of very large cylindrical mesopores. A combination of a commercially available triblock copolymer Pluronic P123 ($EO_{20}PO_{70}EO_{20}$) with a judiciously chosen micelle swelling agent (cyclohexane and 1,3,5-triisopropylbenzene) was used as a micellar template, and the initial step of the synthesis was performed at temperature between 10 and 18 °C, followed by a hydrothermal treatment at 100–150 °C. The PMOs were characterized using small-angle X-ray scattering (SAXS), nitrogen adsorption, transmission electron microscopy, and solid-state ^{29}Si NMR. For all PMO compositions, the formation of 2-D hexagonal structures with (100) interplanar spacing, d_{100}, up to 21–26 nm was achieved, which is at least seven nanometres larger than d_{100} reported earlier for any PMO. The nominal (BJH) pore diameters up to 20–27 nm were achieved for the considered compositions of PMOs with 2-D hexagonal ordering, while even larger pore sizes were sometimes attained for disordered or weakly ordered structures. The mesopores exhibited constrictions or narrow entrances that were widened by increasing the hydrothermal treatment temperature. The pore diameter tended to increase as an initial synthesis temperature decreased, allowing for the pore size adjustment, but the useful temperature range depended on the bridging group. The present work suggests that the low-temperature micelle-templated synthesis with judicious selected swelling agents is a general pathway to ultra-large-pore 2-D hexagonal PMOs with both aliphatic and aromatic bridging groups.

Introduction

The development of porous organosilicas with organic groups homogenously distributed in silica-based frameworks was a breakthrough in the synthesis of high-surface-area porous inorganic–organic hybrid materials.[1,2] The resulting hybrids, which are derived from bis(trialkoxysilyl)organic or multi-(trialkoxysilyl)organic precursors, can be considered as derivatives of silica in which some of the siloxane (Si–O–Si) bridges are replaced Si–R–Si bridges, where R is an organic group. This architecture offers a wealth of opportunities in tailoring physical and chemical properties of materials due to the possibility of incorporation of a variety of bridging organic groups. The discovery of the micelle-templating approach to the synthesis of well-defined mesoporous materials[3–5] led to another breakthrough in the synthesis of the aforementioned organosilicas, endowing them with periodic nanopore structures of well-defined morphology, and uniform pore diameter.[6–9] The resulting materials, commonly referred to as periodic mesoporous organosilicas (PMOs),[10–17] have attracted much attention due to their characteristic surface properties,[7,17] atomic-scale crystallinity[18,19] and other interesting properties, such as controlled hardness and low dielectric constant.[17,20,21] In particular, PMOs were found promising as low-dielectric-constant (low-*k*) materials,[17,20,21] templates for nanostructures,[22] catalysts,[23–25] adsorbents[26,27] and media for immobilization of biomolecules.[28,29]

PMOs have been synthesized with a variety of bridging organic groups, including short saturated aliphatic linkages (methylene, –CH_2–, ethylene, –CH_2–CH_2– and their mono- or disubstituted derivatives)[6–8,30–32] and unsaturated carbon chains (ethenylene, –CH=CH–),[7,8] longer chain-like bridges with heteroatoms,[33] as well as aromatic bridges (including 1,4-phenylene, –C_6H_4–, biphenylene, –C_6H_4–C_6H_4– and their derivatives, as well as 2,5-thiophene, –C_5H_4S–).[9,18,19] In addition to the above two-point-attachment bridges, a variety of more complicated structural units, including aromatic,[34] heteroatom-containing cyclic and multicyclic,[21,35–37] branched[38] and dendritic moieties,[39] were successfully incorporated in PMOs. An additional structural diversity was achieved through co-condensation of bridged organosilanes with one another,[40] or with non-bridged organotrialkoxysilanes (the resulting materials were dubbed bi-functional PMOs, BPMOs).[26,41–43] Moreover, the co-condensation of the bridged organosilanes with silica precursors opened an opportunity to "dilute" organic groups in the framework[8] or to incorporate bridging groups that are not suitable (or not envisioned) to afford a sustainable porous structure.[44–46] However, in the case of the latter co-condensation strategy, the presence of organic groups in the periodic framework (rather than on the surface of pure-silica framework or in separate

[a]*Center for Engineered Polymeric Materials, Department of Chemistry, College of Staten Island, City University of New York, 2800 Victory Boulevard, Staten Island, New York, 10314, USA*
[b]*Graduate Center, City University of New York, 365 Fifth Avenue, New York, New York, 10016, USA. E-mail: Michal.Kruk@csi.cuny.edu*

† Electronic supplementary information (ESI) available: The table with structural parameters derived from SAXS and adsorption data, and figures with experimental SAXS patterns, nitrogen adsorption isotherms, pore size distributions, and TEM images. See DOI: 10.1039/c0jm01170c

non-mesostructured domains) is difficult to ascertain.[15] PMOs can also be doped with heteroatoms (Al,[47] Ti,[23,24] and V[25]) in a manner similar to that for pure-silica materials.

In addition to the chemical composition diversity, a variety of nanoscale structure types have been achieved for PMOs, including a 2-dimensional (2-D) hexagonal structure with cylindrical pores,[6] 3-dimensional hexagonal ($P6_3/mmc$),[6] cubic $Pm3n$,[31] body-centered cubic ($Im3m$),[48] and face-centered cubic ($Fm3m$)[49,50] structures with spherical pores as well as a gyroidal ($Ia3d$)[51] structure of approximately cylindrical pores with intersections. The structure type can be controlled to an appreciable extent by the selection of suitable single surfactant or mixed surfactant template.[52,53]

While the framework composition of PMOs was found highly tailorable, their pore size was found much less adjustable than it can be expected on the basis of the studies of pure-silica counterparts.[3,54–59] The pore size of PMOs was tailored by using surfactant molecules of different size, for instance, alkylammonium surfactants of different chain length,[60–63] oligomeric surfactants,[64] and block copolymers[29,36,47,65–78] (in which case a hydrothermal treatment was also found suitable to tune the pore size[67,76]), affording cylindrical and spherical mesopores of diameters from ~2 to 10 nm.[47,67,69] In comparison, the templating with commercially available and custom-made surfactants affords ordered mesoporous silicas with cylindrical pores of diameter from 2 to at least 16 nm,[3,54,55,79,80] and spherical pores of diameter up to 31 nm.[56,57,81] Moreover, the use of micelle swelling agents, which in the case of ordered mesoporous silicas allows one to obtain cylindrical and spherical pores of diameter up to 26–27 nm,[58,59] typically afforded organosilicas that had disordered (or poorly ordered) enlarged pores,[28,49,82–85] or heterogeneous mesoporous structures with a fraction of ordered large-pore domains.[86] A successful swelling-agent-based low-temperature synthesis of well-ordered large-pore PMO with $Fm3m$ structure of spherical mesopores of diameter up to ~15 nm is a notable exception,[87] while other well-ordered PMOs synthesized in the presence of swelling agents had moderate pore diameters.[29,53,88,89] Our literature survey indicates that in the case of PMOs with well-ordered 2-D hexagonal structure of cylindrical mesopores, the largest pore diameter was ~10 nm,[69,71] and the largest (100) interplanar spacing, d_{100}, was 13–14 nm.[36,39] It should be noted that d_{100} multiplied by 1.155 provides the unit-cell parameter that is equal to the distance between the pore centers in 2-D hexagonal structure. In contrast, 2-D hexagonal silicas with pore diameters and d_{100} interplanar spacings up to 26 nm were reported.[59,90] Likewise, pore sizes reported for PMOs with spherical mesopores[87] were much lower than those for pure-silica materials.[58,81] Therefore, there is a clear need for new approaches to the pore size engineering for PMOs to overcome the limitations discussed above.

Recently, new opportunities emerged in the micelle-expander-based synthesis of large-pore ordered mesoporous silicas. The use of appropriate swelling agents (hexane and TMB) at sub-ambient initial temperature (~15 °C) afforded large-pore SBA-15 silica (LP-SBA-15) with cylindrical mesopores up to ~15 nm[91] and LP-FDU-12 silica with $Fm3m$ structure of spherical mesopores of diameter up to ~27 nm.[58] In the latter case, the pore diameter was found to increase as the initial synthesis temperature decreased from 23 to 14–15 °C, thus allowing one to adjust the pore diameter through the control of the initial synthesis temperature. The TMB-based low-temperature synthesis of $Fm3m$ structures of spherical mesopores was extended on ethylene-bridged PMO, and in particular, the temperature lowering led to the increase in the unit-cell parameter and pore size,[87] but in comparison to LP-FDU-12 silica, the PMO had somewhat smaller unit-cell size and much smaller pore diameter (~15 nm). Our studies of LP-SBA-15 and LP-FDU-12 silicas[92,93] indicated that the amounts of the swelling agents (hexane or TMB) solubilized in the block copolymer micelles were quite small. This finding prompted us to seek swelling agents that would solubilize in micelles to a more significant extent than the swelling agents mentioned above, yet not in excessive amount,[59] which is known to lead to foam-like[94] or otherwise disordered products.[95] Based on earlier studies[96,97] of solubilization of organic compounds in micelles and on their extrapolation within families of similar compounds, 1,3,5-triisopropylbenzene (TIPB) and cyclohexane were identified[59] as promising swelling agents in conjunction with commercially available Pluronic P123 ($EO_{20}PO_{70}EO_{20}$) triblock copolymer surfactant, which is the most common copolymer template for 2-D hexagonal materials, including SBA-15 silica[54,98] and PMOs.[66,68,74,76] Cyclohexane is particularly interesting, because it is a cost-effective, common reagent and solvent. The use of a moderate amount of cyclohexane afforded well-ordered large-pore SBA-15 with d_{100} = ~13 nm, whereas the use of its large amount led to a disordered large-pore (~20 nm) product, confirming that cyclohexane is a potent swelling agent. The use of TIPB afforded SBA-15 silica with pore diameters from 10 to 26 nm,[59] thus achieving a major advance in the synthesis of this important material. Herein, it is reported that the application of cyclohexane and TIPB in combination with Pluronic P123 provides a simple and versatile route to families of 2-D hexagonal ultra-large-pore PMOs with aliphatic and aromatic bridging groups in the framework and with nominal (BJH) pore diameters from 12 nm to 20–27 nm, which corresponds to actual pore diameters approaching 20 nm.

Materials and methods

Synthesis of methylene-bridged PMO

In a typical experiment, 2.40 g of Pluronic P123 were combined with 84 ml of 1.30 M HCl solution followed by mechanical stirring until the whole polymer dissolved completely at 15.00 °C (or other temperature selected from 12.00–17.00 °C range). Then premixed bis(triethoxysilyl)methane, BTEM (Gelest Inc.), and 13.0 ml cyclohexane were added. The molar composition of the reaction mixture was BTEM/P123/cyclohexane/HCl/H_2O = 0.50 + x/0.0168/4.88/4.42/186, with x = 0.30 (preferred composition), 0.20 or 0.40 (x = 0 would correspond to the Si/P123 molar ratio most commonly used in SBA-15 silica synthesis[59,98]). The solution was stirred for one day at the initial temperature (15.00 °C or other) and subsequently hydrothermally treated for 2 days at 100 °C (in closed polypropylene (PP) bottle) or a higher temperature (130 or 150 °C; in Teflon® lined autoclave). The resulting as-synthesized sample was filtered, washed with deionized water, and dried at ~60 °C under vacuum. Finally, the material was calcined under air at 300 °C (heating ramp 2 °C min^{-1}) for 5 h to remove the

surfactant (which can also be removed by calcination under N_2 at 300 °C or by Soxhlet extraction with ethanol).

Synthesis of ethylene-bridged PMO

0.60 g of Pluronic P123 was combined with 21 ml of 1.30 M HCl solution followed by mechanical stirring until the surfactant dissolved completely at a temperature of 15.00 °C (or other temperature from 10.00–15.00 °C range). Then premixed bis-(trimethoxysilyl)ethane, BTME (Gelest Inc. or Aldrich) or bis-(triethoxysilyl)ethane, BTEE (Gelest Inc.), and 3.25 ml cyclohexane were added. The molar composition of the reaction mixture was BTME (or BTEE)/P123/cyclohexane/HCl/H_2O = 0.50 + x/0.0168/4.88/4.42/186, with x = 0.40, 0.60 (preferred composition), 0.70, 1.00 and 1.50 for BTME, and 0.40 for BTEE. The solution was stirred for one day at the initial temperature and subsequently hydrothermally treated for 2 days at 100 °C in closed PP bottle. The as-synthesized sample was filtered, washed and dried as described above. Finally, the surfactant was removed by Soxhlet extraction with ethanol (or calcination under N_2 at 300 °C, if so noted).

Synthesis of ethenylene-bridged PMO

The synthesis was performed using bis(triethoxysilyl)ethylene (BTEEn) as a precursor in a way analogous to that described above for BTME. The molar composition was BTEEn/P123/cyclohexane/HCl/H_2O = 0.50 + x/0.0168/4.88/4.42/186, with x = 0.40 (or 0.70, if so noted). The surfactant was removed by extraction.

Synthesis of phenylene-bridged PMO

0.60 g of Pluronic P123 was combined with 21 ml of 1.30 M HCl solution followed by mechanical stirring until the surfactant dissolved completely at an initial temperature of 14.00–18.00 °C. Then, premixed 1.95 ml of 1,4-bis(triethoxysilyl)benzene, BTEB (Gelest, Inc. or Aldrich), and 1.2 ml (or 0.6 ml, if so noted) 1,3,5-triisopropylbenzene (TIPB) were added. The molar composition was BTEB/P123/TIPB/HCl/H_2O = 0.50 + x/0.0168/0.79 (or 0.40)/4.42/186, with x = 0.30. The solution was stirred at the selected initial temperature for one day and then hydrothermally treated in PP bottle at 100 °C for 2 days. As-synthesized material was filtered, washed and dried as described above. Finally, the template was removed from the material by Soxhlet extraction with ethanol and calcination under air at 250 °C[76] (or calcination under N_2 at 300 °C, if so noted).

Measurements

Small-angle X-ray scattering (SAXS) patterns were recorded on Bruker Nanostar U SAXS/wide-angle X-ray scattering (WAXS) instrument equipped with a rotating anode X-ray source and a 2-D detector Vantec 2000. The instrument was in a high flux configuration and the flight path was ~73 cm. Samples were placed in a hole of a sample holder and secured on both sides using a Kapton tape. Nitrogen adsorption measurements were carried out at −196 °C on Micromeritics ASAP 2020 volumetric gas adsorption analyzers. The samples were outgassed at 140 °C in the port of the adsorption analyzer before the analysis. Transmission electron microscopy (TEM) images were recorded on FEI Tecnai G2 Twin microscope operated at an accelerating voltage of 120 kV. The sample was sonicated in ethanol, then drop-cast on carbon-coated copper grid. The ethanol was allowed to evaporate under air before the TEM imaging. Cross-polarization magic angle spinning (CP MAS) ^{29}Si NMR spectra were acquired using Varian INOVA 300 wide bore spectrometer. The operating frequency was 59.6 MHz. Samples were packed into a 5 mm zirconia rotor, loaded into a 5 mm Doty XC-5 CP/MAS probe and spun at 6–8 kHz. 1000–2000 Scans were acquired based on the sensitivity of the sample.

Calculations

The BET specific surface area was determined from nitrogen adsorption isotherm data in a relative pressure range 0.04–0.2.[99] The total pore volume was determined from the amount adsorbed at a relative pressure of 0.99.[99] The pore diameter was determined from the adsorption branch of the isotherm using the BJH method.[100,101] The micropore volume was calculated using the α_s plot method with LiChrospher Si-1000 silica.[99,102]

Results and discussion

Methylene-bridged PMO

As mentioned above, cyclohexane was predicted as a promising swelling agent for the Pluronic-P123-templated synthesis of mesoporous materials and was found useful for the SBA-15 silica synthesis.[59] Herein, it is shown that cyclohexane is even more suitable, and in fact, very powerful, in the synthesis of large-pore PMOs, if it is added in large quantity to the synthesis mixture. Under such conditions, methylene-bridged PMO was obtained whose SAXS pattern (Fig. 1) featured peaks indexable as (100), (110), (200), and (300) reflections of 2-D hexagonal structure of cylindrical mesopores with the (100) interplanar spacing, d_{100}, of 22 nm (Table 1), which is ~50% larger than the largest d_{100} reported earlier for any 2-D hexagonal PMO. As seen from TEM, particles of the PMO commonly had a rod-like morphology (Fig. S1†), and series of parallel uniformly spaced stripes (which are known to be side projections of a honeycomb) were readily noticeable along the rods (Fig. 2 and S1†), showing

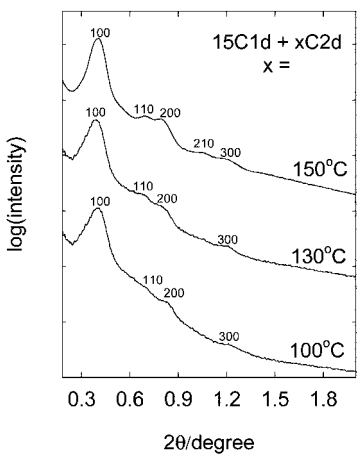

Fig. 1 SAXS patterns for methylene-bridged PMOs synthesized at initial temperature of 15 °C followed by hydrothermal treatment for two days at different temperatures.

Table 1 Structural properties of PMOs[a]

Sample (bridge, initial temp.)	d_{100}/nm	S_{BET}/ m^2g^{-1}	V_t/ $cm^3\ g^{-1}$	V_{mic}/ $cm^3\ g^{-1}$	w_{BJH}/ nm
Methylene, 17 °C	21.3	1140	1.39	0.24	18.5
Methylene, 15 °C	22.1	1120	1.56	0.21	23.3
Methylene, 14 °C	22.1	1220	1.50	0.32	19.7
Methylene, 13 °C	30[c]	1180	1.27	0.35	23.9
Methylene, 12 °C	—[d]	1170	1.12	0.40	31
Ethylene, 15 °C	16.8	498	0.59	0.13	13.7
Ethylene, 12 °C[b]	19.6	705	0.62	0.25	16.7
Ethylene, 11 °C	24.2	452	0.44	0.15	21.6
Ethylene, 10.75 °C[b]	25.6	631	0.52	0.23	22.2
Ethylene, 10.5 °C[b]	~28[d]	626	0.47	0.26	26.0
Ethylene, 10 °C	—[e]	136	0.23	0.02	—[f]
Ethenylene, 15 °C	14.6	263	0.50	0.03	11.9
Ethenylene, 12 °C	16.8	322	0.45	0.06	14.3
Ethenylene, 11 °C	21.3	691	0.71	0.24	20.1
Ethenylene, 10.5 °C	22.1	459	0.52	0.14	21.2
Ethenylene, 10 °C	~22[d]	69	0.17	0.01	22
Phenylene, 18 °C[g]	15.0	609	0.60	0.19	12.0
Phenylene, 18 °C	17.3	646	0.68	0.21	14.4
Phenylene, 17 °C	19.6	669	0.89	0.19	17.2
Phenylene, 16 °C	22.1	722	0.80	0.24	20.3
Phenylene, 15.5 °C	26.4	646	0.69	0.23	27.5
Phenylene, 15 °C	~24[d]	664	0.77	0.23	25.1
Phenylene, 14 °C[b,g]	—[e]	466	0.40	0.18	—[f]

[a] Notation: d_{100}, (100) interplanar spacing for extracted or/and calcined sample. S_{BET}, BET specific surface area; V_t, total pore volume; V_{mic}, micropore volume; and w_{BJH}, BJH pore diameter. [b] Sample was calcined at 300 °C under N_2. [c] Estimated by tentatively assigning the first peak on SAXS pattern as (100) peak. [d] Could not be valuated accurately due to the presence of shoulder on SAXS pattern. [e] Could not be evaluated due to absence of peak on SAXS pattern. [f] No clear peak on the mesopore size distribution. [g] Amount of TIPB used was 0.6 ml per 0.6 g of P123.

that the channels run along the rods. Such a particle morphology makes it difficult to see honeycomb arrangements of the pores, but they were also observed (Fig. 2). The surface of the rods appeared to be rough, suggesting that the rods were covered by channels circling around the rods or by some other less well defined porous structure. The methylene-bridged PMO was further characterized by nitrogen adsorption to determine its textural properties. The adsorption isotherm (Fig. 3) showed a steep capillary condensation step centered at a high relative pressure of ~0.91, thus indicating the presence of very large mesopores. The PMO exhibited a high BET specific surface area (1120 $m^2\ g^{-1}$) and a large total pore volume (1.56 $cm^3\ g^{-1}$). The pore size distribution (PSD) was quite narrow (Fig. 3) and featured a maximum at a nominal (BJH) pore diameter of ~23 nm, whereas an actual pore diameter was evaluated to be 20 nm (by using eqn (1) from ref. 59 and confirmed by comparing the nominal (BJH) pore diameter with nominal and corresponding actual pore sizes reported in ref. 59), which is about two times larger than the largest pore size reported earlier for a 2-D hexagonal PMO. The pore wall thickness can be estimated to be ~6 nm, which is larger than that of SBA-15 silica synthesized under similar conditions.[59,103]

The ultra-large cylindrical mesopores were accessible through constrictions, as seen from a broad adsorption–desorption hysteresis loop (Fig. 3) that closed primarily at the lower pressure limit of adsorption–desorption hysteresis (p/p_0 of 0.50), thus suggesting that the constrictions were of diameter below 5 nm.[104] Similar constrictions were observed for large-pore SBA-15 prepared at low temperature without a hydrothermal treatment,[59,92] and were shown to be reduced or fully eliminated by increasing the temperature of the hydrothermal treatment.[59,92] In the case of the considered PMO, the accessibility of the pore channels was improved by applying the hydrothermal treatment at 130–150 °C, as seen from nitrogen adsorption isotherms exhibiting the capillary evaporation above the lower limit of hysteresis (Fig. 3). Concomitantly, the pore diameter increased slightly as the temperature was increased from 100 to 130 or 150 °C (Fig. 3; BJH pore diameter up to 25 nm, see Table S1†). It should be noted that the sample treated at 100 °C (Table 1) and

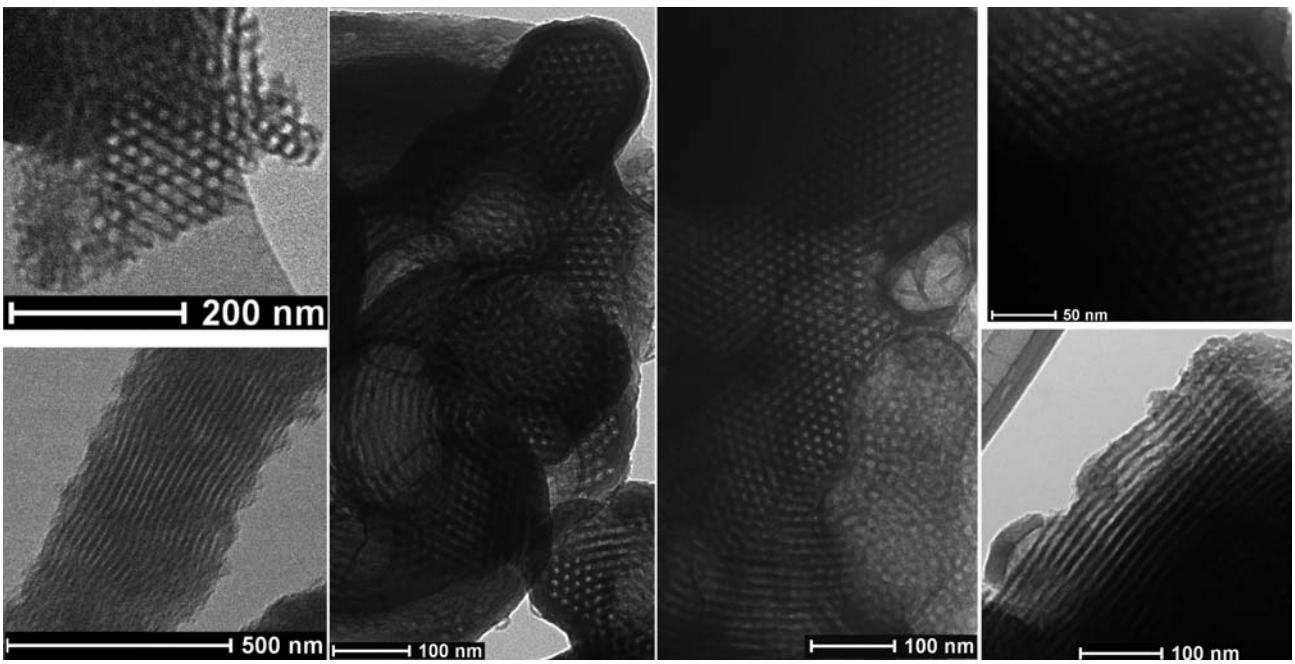

Fig. 2 TEM images of PMOs with (left) methylene, (middle left) ethylene (as-synthesized), (middle right) ethenylene, and (right) phenylene bridging groups.

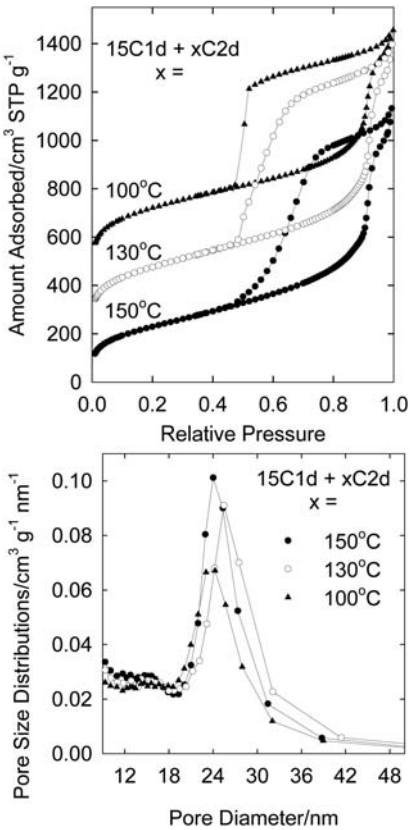

Fig. 3 Nitrogen adsorption isotherms (top) and pore size distributions (bottom) for methylene-bridged PMOs synthesized at initial synthesis temperature of 15 °C followed by hydrothermal treatment for two days at different temperatures. Isotherms were offset vertically by 200 and 400 cm^3 STP g^{-1} for samples hydrothermally treated at 130 and 100 °C, respectively.

130 °C (Table S1†) came from the same synthesis mixture, but the sample treated at 150 °C came from another synthesis (which afforded $w_{BJH} = 21.8$ nm for the material treated at 100 °C). It is noteworthy that even after the treatment at such high temperatures, the hysteresis loops on the isotherms for PMOs were appreciably broader than those for materials with mesopores free of constrictions,[59] indicating that it is difficult to fully eliminate the constrictions. The latter can be present either inside the mesopores (as "plugs")[105,106] or at their entrances, this possibility being suggested by TEM observations of ethylene-bridged and ethenylene-bridged organosilicas (see below). ^{29}Si NMR indicated that calcination at 300 °C under air, which was typically used in our study to remove the template from methylene-bridged PMO led to a slight cleavage of Si–C bonds, as Q sites (between −90 and −110 ppm) appeared in addition to T sites (T_3 at −69 ppm) (see Fig. S2†). However, the surfactant removal can also be achieved *via* calcination at 300 °C under N_2 or ethanol extraction (see SAXS, adsorption and pore size data in Fig. S2†) with the retention of the integrity of Si–C bonds, as seen from the absence of signal corresponding to Q sites in ^{29}Si NMR (Fig. S2†). It is also determined that the hydrothermal treatment at 150 °C did not lead to the cleavage of Si–C bonds (see Fig. S3†).

For the methylene-bridged PMO, the ultra-large-pore structure was found to form at an organosilica-precursor/surfactant ratio that corresponded to a 60% higher Si/P123 molar ratio than that typically used in the SBA-15 synthesis. Moderate deviations from this ratio afforded materials with much smaller interplanar spacings (Table S1 and Fig. S4†), which provide the basis for a coarse adjustment of the pore size. On the basis of our previous study of large-pore SBA-15 silica templated by Pluronic P123 swollen by TIPB,[59] it was expected that the lowering of the initial synthesis temperature would lead to the unit-cell enlargement and the pore diameter increase. However, the ultra-large-pore methylene-bridged PMO was not particularly amenable to the structural adjustment. The pore diameter and unit-cell size exhibited little variation within the 14–17 °C range (see Table S1 and Fig. S5†). As the temperature was decreased to 13 °C, the pore diameter somewhat increased, but the SAXS pattern became poorly resolved, having only one peak whose position corresponded to very large repeating distance of ~30 nm. Further temperature decrease to 12 °C led to a marked pore diameter increase, but the SAXS pattern merely exhibited a shoulder at very low angles, showing the loss of structural uniformity.

Ethylene- and ethenylene-bridged PMO

Cyclohexane was also found to be a powerful swelling agent for the synthesis of ethylene- and ethenylene-bridged PMOs, but in these cases, the unit-cell size was readily adjusted by selecting the initial synthesis temperature (resembling the synthesis of large-pore SBA-15 silica in the presence of TIPB) and was largely independent of the organosilica-precursor/surfactant ratio. When the initial step of the synthesis was performed at 15 °C, the SAXS pattern for ethylene-bridged PMO (Fig. 4, top) showed five peaks, which can be identified as (100), (110), (200), (210) and (220)/(310) reflections of 2-D hexagonal structure with d_{100} = 16.8 nm. The corresponding SAXS pattern for ethenylene-bridged PMO (Fig. 4, bottom) showed four peaks, which were identified as (100), (110), (200) and (220)/(310) reflections of 2-D hexagonal structure with d_{100} = 14.6 nm. TEM confirmed the structures of both PMOs (Fig. 2), but also suggested the presence of non-mesoporous (non-templated) domains (for ethenylene-bridged PMO) or apparently non-mesoporous envelopes around particles (for ethylene-bridged PMO, see Fig. 2). Nitrogen adsorption isotherms (Fig. 5) for the considered PMOs showed steep capillary condensation steps (indicative of narrow PSDs) centered at relative pressures of 0.85 and 0.83, thus suggesting large pore sizes. The corresponding PSDs had maxima at 14.1 and 12.4 nm, respectively (Fig. 6), which are larger than the largest pore diameters reported previously for any 2-D hexagonal PMO. For ethylene-bridged PMO, the unit-cell size and the pore size were found to be largely independent of the BTME/P123 molar ratio. As the relative amount of the organosilica precursor was increased and eventually more than doubled, the 2-D hexagonal structure retained quite constant d_{100} (16.1–18.0 nm) and similar degree of structural ordering, as seen from the occurrence of five reflections on SAXS patterns (see Fig. S6 and Table S1†). The lowest BTME/P123 ratio afforded the broadest PSD. On the other hand, the samples prepared at the two highest BTME/P123 ratios had non-mesoporous domains clearly visible

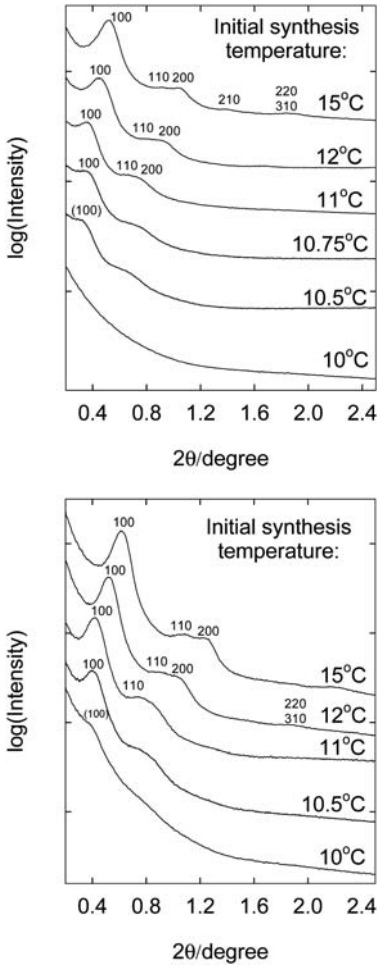

Fig. 4 SAXS patterns for extracted (unless otherwise noted) ethylene-bridged (top) and ethenylene-bridged PMOs (bottom) synthesized at different initial temperatures. Ethylene-bridged PMOs synthesized at 10.5, 10.75, and 12 °C were calcined under N_2 at 300 °C.

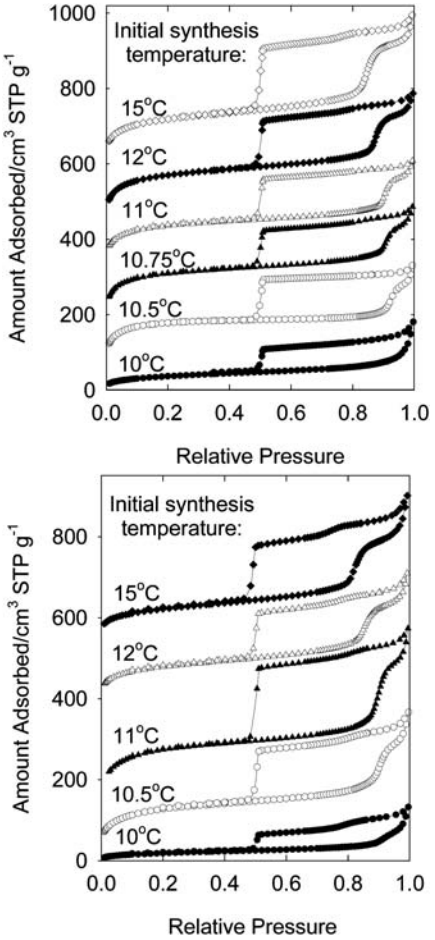

Fig. 5 Nitrogen adsorption isotherms for extracted (unless otherwise noted) PMOs synthesized at different initial temperatures: (top) ethylene-bridged PMOs (samples synthesized at 10.5, 10.75, and 12 °C were calcined under N_2 at 300 °C) and (bottom) ethenylene-bridged PMOs. The isotherms were offset vertically by 130, 310, 370, and 580 cm^3 STP g^{-1} for samples synthesized at initial temperature of 10.75, 11, 12, and 15 °C, respectively (top). The isotherms were offset vertically by 80, 390, and 550 cm^3 STP g^{-1} for samples synthesized at initial temperature of 11, 12, and 15 °C, respectively (bottom).

in TEM, while such features were not apparent in the case of the lowest ratio. The intermediate ratios might have afforded a fraction of non-mesoporous organosilica deposited on the outer surface of the ordered nanoporous particles, as dark envelopes around the particles were observed (see Fig. 2). In addition, a small amount of worm-like or foam-like regions was seen for the lowest and intermediate BTME/P123 ratios. For the subsequent studies, the second lowest BTME/P123 ratio was chosen. The effect of BTEEn/P123 ratio on the ethenylene-bridged PMO was also rather minor (see Fig. S7 and Table S1†). Clearly, the synthesis of large-pore PMOs with bridges composed of two carbon atoms proceeded in a similar manner for different proportions of the organosilica precursor to the surfactant, unlike the synthesis of methylene-bridged PMO that was very sensitive to this factor. The integrity of the ethylene and ethenylene bridges after solvent extraction was confirmed by ^{29}Si NMR (Fig. S6 and S7†).

The initial synthesis temperature played a crucial role in determining unit cell dimensions and pore sizes for the ethylene- and ethenylene-bridged PMOs (Table 1 and Fig. 4–6). The lowering of the initial temperature from 15 to 10.75 °C for the ethylene-bridged PMO led to d_{100} increase from 16.8 to 26 nm, the latter being similar to the highest d_{100} reported for SBA-15 silica.[59] As temperature decreased, the SAXS patterns became less resolved. TEM confirmed a 2-D hexagonal structure for the samples synthesized in the 10.75–15.00 °C range (see Fig. 7), although samples prepared at 10.75–11.00 °C also contained characteristic structures seen predominantly for 10.50 °C sample (see below). The SAXS pattern for the sample prepared at 10.5 °C was somewhat less resolved and TEM no longer provided evidence for 2-D hexagonal structure, although cylindrical mesopores that were embedded in apparently non-mesoporous framework were clearly seen (Fig. S8†). These pore channels tended to be parallel to one another and in some cases formed monolayer structures, which allowed us to clearly see the elongated shape of individual mesopores, which were quite uniform in diameter, straight or curved. Hemispherical ends of the channels were clearly seen, so were circular pore openings at the edge. The observed morphology of the channels is expected to closely reflect the shape of the micelles that originally templated

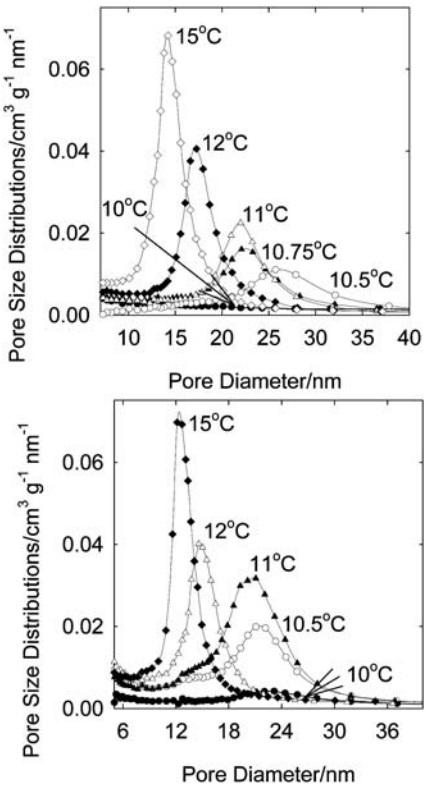

Fig. 6 Pore size distributions for extracted (unless otherwise noted) ethylene-bridged (top) and ethenylene-bridged PMOs (bottom) synthesized at different initial synthesis temperature. Ethylene-bridged PMOs synthesized at 10.5, 10.75, and 12 °C were calcined under N_2 at 300 °C.

the material, thus providing a unique insight into the micellar structures. It should be noted that the mesopore voids are expected to reflect primarily the hydrophobic core of the block copolymer micelle (in this case, PPO domains swollen with cyclohexane), whereas the space once occupied by PEO blocks is not expected to be readily visible, because PEO chains or strands of chains are expected[107] to be occluded in the organosilica matrix, as they template disordered (primarily microporous) network of pores in the organosilica walls. The fact that the channels, including their ends, seemed to be embedded in the apparently non-mesoporous framework may be the reason why the large mesopores of this PMO were accessible to N_2 molecules through narrow constrictions, as seen from nitrogen adsorption data (Fig. 5) that will be discussed below. Namely, the micropores (or small mesopores) in the framework may constitute primary access pathways to the uniform mesopores. As was already discussed for methylene-bridged PMO and will be discussed below for other PMOs, their mesopores exhibited narrow entrances as well, so the capped mesopore ends may provide an explanation alternative to that involving plugged mesopore interiors known for some silica-based materials[105,106] and suggested also for some PMOs.[72]

As discussed above for ethylene-bridged PMO, the 2-D hexagonal structure persisted to 10.75 °C and the cylindrical pore shape was retained even at 10.50 °C. The largest nominal (BJH) pore diameter for 2-D hexagonally ordered PMO was 22 nm (10.75–11.00 °C synthesis), which is about two times larger than the largest pore size of ethylene-bridged PMOs reported earlier. In addition, the largest nominal pore diameter for our material with a confirmed cylindrical pore shape was 26 nm. As in the case of methylene-bridged PMO, the adsorption isotherms for ethylene-bridged PMOs exhibited broad hysteresis loops with capillary evaporation primarily at the lower limit of adsorption–desorption hysteresis, indicating the existence of constrictions of diameter not larger than 5 nm in the mesopores.

A similar temperature effect was observed for ethylene-bridged PMOs synthesized using bis(triethoxysilyl)ethane (BTEE) precursor, which is a more cost-effective and benign alternative to BTME, differing in the presence of ethoxy groups instead of methoxy groups that hydrolyze faster. BTEE-derived PMOs were highly ordered (see Fig. S9†), and their pore diameters (Table S1†) increased as an initial synthesis temperature decreased from 15.00 to 11.00 °C, following the trend observed for BTME-derived PMOs, although the latter had somewhat larger interplanar spacing. These results point to a minor influence of the kind of the hydrolyzable group in the organosilica precursor on the formation of 2-D hexagonal PMOs templated by P123 swollen by cyclohexane.

The ethenylene-bridged PMOs exhibited a temperature behavior quite similar to that of the ethylene-bridged PMOs. The (100) interplanar spacing increased from 14.6 to 22.1 nm as the initial synthesis temperature was lowered from 15.00 to 10.50 °C, while the SAXS patterns were quite well resolved for all samples (Fig. 4), even for the one prepared at 10.50 °C. However, there was no significant increase in d_{100} between 11.00 and 10.50 °C. The sample synthesized at 11.00 °C still exhibited 2-D hexagonally ordered structures of cylindrical mesopores (Fig. 7), but

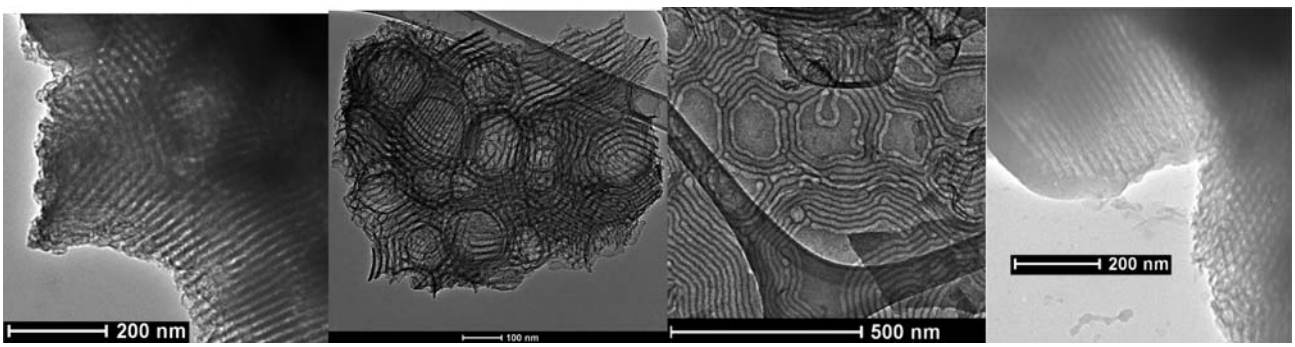

Fig. 7 TEM image of (left) extracted ethylene-bridged PMO synthesized at initial temperature of 11 °C; middle left and right: extracted ethenylene-bridged PMO synthesized at 11 °C and right: phenylene-bridged PMO synthesized at 15.5 °C (calcined under N_2 at 300 °C).

also featured spectacular maze-like structures (Fig. 7; a larger area is shown in Fig. S10†), whose images provide insight into the morphology of the mesopores as well as of the micelles, as discussed above. A further lowering of the initial temperature to 10.00 °C led to a material with a rather featureless SAXS pattern. The inferences from SAXS were mirrored by nitrogen adsorption data (Fig. 5), which revealed uniform mesoporous structures with narrow PSDs (Fig. 6) and the increase in the pore diameter for samples synthesized at initial temperatures between 15.00 and 11.00 °C, with additional minor increase in nominal (BJH) pore diameter (from 20.4 to 21.5 nm) as the temperature decreased to 10.50 °C. This limiting pore diameter is about two times larger than the largest pore diameters documented for 2-D hexagonal ethenylene-bridged PMOs. The lowering of temperature to 10.00 °C did not bring any appreciable pore size increase, while the height of the PSD peak decreased dramatically, confirming a diminished propensity to the formation of a uniform nanostructure at 10 °C. The presence of constrictions in the mesopore structure was inferred from the shape of the hysteresis loops on nitrogen adsorption isotherms (Fig. 5). One can conclude that for both ethylene- and ethenylene-bridged PMOs, there is an appreciable range (from 15 down to 10.50–10.75 °C) in which the temperature decrease brings about the unit-cell size and pore diameter increase, while the periodic nanostructure is no longer a major product in the case where the initial temperature is lowered to 10 °C.

The results discussed above for methylene-, ethylene- and ethenylene-bridged PMOs point to a broad applicability of the P123/cyclohexane combination in the synthesis of large-pore PMOs with aliphatic bridges. Additional evidence pointing to that comes from our work on the synthesis of PMO with an aliphatic bridging group with a double bond on the middle carbon atom using $(CH_3O)_3Si–CH_2–C(=CH_2)–CH_2–Si(OCH_3)_3$ as a precursor. Under optimized conditions, materials with SAXS patterns featuring a strong peak (the corresponding interplanar spacing was 15–16 nm) and a shoulder, and with fairly large pores (14–15 nm) were recovered (see Fig. S11†). TEM revealed an ordered, but heterogeneous structure, including features characteristic of 2-D hexagonal structure (predominant) with some evidence of the presence of multi-layer vesicles/onions and a 3-D cubic structure of spherical mesopores. Unfortunately, ^{29}Si NMR indicated a complete cleavage of Si–C bonds and conversion to pure silica, which can be related to the similarity of the bridging group to an allyl moiety that can be used as a hydrolyzable group.[108] However, one can speculate that the periodic structure formed before any major cleavage of the bridging groups took place, because in the case of high content of cyclohexane in the synthesis mixture, silica derived from TEOS had a much less ordered, larger-pore structure.[59] Therefore, the above results for the new organosilica precursor appear to confirm the general applicability of the P123/cyclohexane pair in the synthesis of large-pore PMOs with aliphatic bridging groups.

1,4-Phenylene-bridged PMOs

The synthesis of large-pore 2-D hexagonal PMO with phenylene bridging groups using Pluronic P123 surfactant in combination with readily available swelling agents (cyclohexane or hexane) was unsuccessful, affording materials with moderate pore diameters (8–9 nm) and devoid of any significant structural ordering. On the other hand, the use of TIPB, which was demonstrated earlier to be an excellent swelling agent for SBA-15 silica[59] afforded a family of large-pore 2-D hexagonal phenylene-bridged PMOs after identification of a proper temperature range. An initial synthesis temperature of 15 °C, which was suitable for the synthesis of LP-FDU-12[58] and LP-SBA-15 silicas,[59] as well as large-pore PMOs with aliphatic bridges (see above), was found to be a lower boundary of the range for the formation of 2-D hexagonal phenylene-bridged PMO. The selection of slightly higher temperatures (15.5–18 °C) allowed us to obtain PMOs with a wide range of interplanar spacings and pore diameters. The SAXS pattern (Fig. 8) for phenylene-bridged PMO synthesized at an initial temperature of 18 °C featured (100), (110), (200), and (210) reflections for 2-D hexagonal structure with $d_{100} = 15.0$ nm. TEM further supported this structural assignment (Fig. 2), although the presence of some bulk (non-nanostructured) domains was also likely based on TEM. ^{29}Si NMR confirmed that the removal of surfactant by extraction followed by calcination under air at 250 °C or by calcination under nitrogen at 300 °C did not lead to any appreciable cleavage of Si–C bonds in the PMO framework (see Fig. S12†). The PMO exhibited an adsorption isotherm (Fig. 8) similar to that discussed above for ethylene- and ethenylene-bridged PMOs, and the nominal (BJH) pore diameter of 12.0 nm (Fig. 8), which is larger than the pore diameter reported earlier for any PMO with 2-D hexagonal structure. The above synthesis was performed with 0.6 ml TIPB per 0.6 g of P123, which is similar to the amount used in ULP-SBA-15 synthesis.[59] The nominal pore diameter was increased to 14.4 nm and d_{100} reached 17.3 nm, when the relative amount of TIPB was doubled (this TIPB/P123 ratio was used for most of the samples discussed below, while a lower ratio was used for samples described in Table S1 and Fig. S12†). With a decrease of the initial synthesis temperature to 15.5 °C, the interplanar spacing increased to 26 nm (as seen from SAXS shown in Fig. 8) and the nominal (BJH) pore diameter increased to 27 nm, while the 2-D hexagonal structure was retained (as seen from SAXS and/or TEM, see illustrative image in Fig. 7). As for other PMO families, the mesopores exhibited constrictions, as seen from broad adsorption–desorption hysteresis loops on the isotherms (Fig. 8). One can conclude that 2-D hexagonal phenylene-bridged PMOs with d_{100} and pore diameter up to two times larger than those reported earlier for this PMO composition were successfully synthesized.

Formation of large-pore PMOs

The successful formation of 2-D hexagonal large-pore PMOs under sub-ambient conditions using Pluronic P123 as a surfactant and cyclohexane or TIPB as a swelling agent follows the predictions applied in selecting a surfactant/swelling-agent combination for the synthesis of ultra-large-pore SBA-15.[59] It was already demonstrated[59,103] that the identity of the hydrolyzable group (ethoxy or methoxy) of the tetraalkoxysilane silica precursor does not have any dramatic effect on the formation of ULP-SBA-15. Similarly, there was no major difference between the results for two different organosilica precursors (BTME and BTEE with methoxy or ethoxy groups, respectively) of ethylene-bridged PMO. On the other hand, the presence and

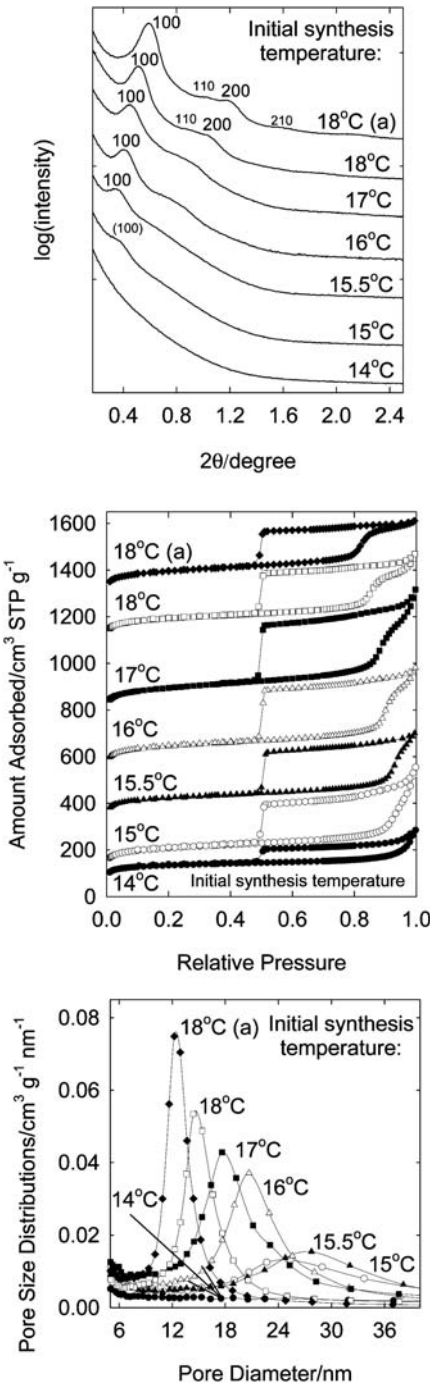

Fig. 8 Top: SAXS patterns for phenylene-bridged PMOs synthesized at different initial temperatures using 1.2 ml TIPB per 0.6 g of P123 (except for sample (a) and sample synthesized at 14 °C, where 0.6 ml TIPB per 1.2 g of P123 was used). Middle: nitrogen adsorption isotherms and bottom: pore size distributions for the considered PMOs. The samples were extracted and calcined at 250 °C under air, except for the sample prepared at 14 °C that was calcined at 300 °C under N_2. Isotherms for the samples synthesized at initial temperatures of 15, 15.5, 16, 17, 18, and 18 °C (0.6 ml TIPB) are offset vertically by 20, 240, 440, 725, 1010, and 1220 cm ^{3} STP g^{-1}, respectively.

identity of the bridging organic group in the precursor and ultimately in the PMO framework have a major effect on the formation of the material and its unit-cell size. Let us consider first the use of a large relative amount of cyclohexane, which is known to afford poorly defined, large-pore pure-silica product.[59] Under these conditions, methylene-bridged PMOs with very large d_{100} and pore diameter formed at a particular organosilica-precursor/P123 ratio, in a quite wide temperature range from 17 down to 14 °C, and with an interplanar spacing and pore diameter increase paralleled by a significant loss of ordering at 13 °C. On the other hand, PMOs with slightly larger, two-carbon-atom bridging groups (ethylene and ethenylene) were formed at temperatures from 15 to 10.5–10.75 °C, and only at the lower limit of this range (10.5–11.0 °C), their unit-cell sizes approached that of the methylene-bridged PMO, which formed a well-ordered nanostructure only at 14 °C or higher. The formation of the PMOs with two-carbon-atom bridges was largely independent of the organosilica-precursor/surfactant molar ratio, unlike in the case of methylene-bridged PMO. Therefore, for a particular surfactant/swelling-agent combination, the formation of an ordered structure as well as its unit-cell and pore dimensions are not merely governed by temperature, but also are significantly influenced by the precursor and/or framework composition. This suggests that the organosilica precursor or more likely, the products of its hydrolysis, mediates the formation of the swollen micelles. The interactions of the organosilica component with the hydrophobic core of the micelles are additionally suggested by the occurrence of the constrictions in the cylindrical mesopores, which may indicate some extent of penetration of the organosilica framework into the hydrophobic domain of the templating micelle. The three-component system (surfactant/swelling agent/organosilica precursor and/or framework) that appears to govern the formation of the large-unit-cell organosilica/surfactant composites is likely to have a unique stability domain in the composition/temperature space, and thus it is not surprising that a small change in the initial temperature or composition may in some cases produce a major change in the structural properties (unit-cell size, pore diameter) of the resulting PMO.

The synthesis of phenylene-bridged PMO using Pluronic P123/TIPB pair can be best compared to the synthesis of LP-SBA-15 using the same surfactant/swelling-agent pair.[59,103] At temperatures where the PMO formed, its (100) interplanar spacing was larger than that for SBA-15 prepared at the same temperature. However, PMO did not form below 15 °C, whereas SBA-15 turned into a disordered ultra-large-pore structure at a much lower temperature (~12 °C). This result confirms the notion that the precursor and/or framework composition influence the formation and dimensions of the swollen micelles.

Conclusions

In the 10–18 °C range, the combination of Pluronic P123 triblock copolymer and cyclohexane or 1,3,5-triisopropylbenzene affords a micellar template for ultra-large-pore 2-D hexagonal periodic mesoporous organosilicas with a variety of framework compositions, including aliphatic and aromatic bridging groups. As the initial synthesis temperature decreases, the unit-cell parameter and the mesopore size tend to increase. The unit-cell enlargement is paralleled by a decrease in the degree of structural ordering and pore size uniformity, eventually reaching the temperature at which disordered materials are obtained, which in some cases still have quite uniform pore diameter. The temperature range at

which the unit-cell parameter and the pore size are adjustable depends on the identity of the bridging group in the PMO precursor. The large cylindrical mesopores of the 2-D hexagonal PMOs exhibit narrow entrances or internal constrictions, which can be widened by increasing the temperature of the hydrothermal treatment, but are difficult to fully eliminate. These observations suggest that the organosilica precursor interacts with the hydrophobic domain of the micellar template (that is, with the swollen PPO domain), mediating the micelle formation or swelling process, perhaps partially cross-linking in the hydrophobic domain. The (100) interplanar spacing up to 21–26 nm achievable for 2-D hexagonal PMOs approaches the upper limit of the d_{100} range reported for SBA-15 silica synthesized using P123/TIPB combination (~26 nm).[59] On the other hand, pore diameters attainable for PMOs were somewhat smaller (up to ~20 nm; nominal (BJH) pore diameter up to 20–27 nm) than those achievable for SBA-15 (up to ~26 nm; nominal (BJH) pore diameter up to ~34 nm), which is related to a larger pore wall thickness of PMOs. The proposed approach of using judiciously chosen swelling agents to mediate the formation of large-pore PMOs at low temperatures was found applicable for PMOs with both aliphatic (saturated and unsaturated) and aromatic bridging groups and is thus expected to be generally applicable for a wide variety of PMOs and related materials. It may also be generalizable for other framework compositions. The novel PMOs with the large pore size and tailorable properties open new opportunities in many applications for which PMOs are contemplated and evaluated.

Acknowledgements

Dr Jianqin Zhuang (CSI) is acknowledged for assistance with NMR measurements. The Imaging Facility at CSI is acknowledged for providing access to TEM. The NSF is gratefully acknowledged for funding the acquisition of SAXS/WAXS system through award CHE-0723028. Acknowledgment is made to the Donors of the American Chemical Society Petroleum Research Fund for partial support of this research (Award PRF #49093-DNI5). BASF is acknowledged for the donation of the Pluronic P123 triblock copolymer.

Notes and references

1 D. A. Loy and K. J. Shea, *Chem. Rev.*, 1995, **95**, 1431–1442.
2 G. Cerveau and R. J. P. Corriu, *Coord. Chem. Rev.*, 1998, **178–180**, 1051–1071.
3 J. S. Beck, J. C. Vartuli, W. J. Roth, M. E. Leonowicz, C. T. Kresge, K. D. Schmitt, C. T. W. Chu, D. H. Olson, E. W. Sheppard, S. B. McCullen, J. B. Higgins and J. L. Schlenker, *J. Am. Chem. Soc.*, 1992, **114**, 10834–10843.
4 C. T. Kresge, M. E. Leonowicz, W. J. Roth, J. C. Vartuli and J. S. Beck, *Nature*, 1992, **359**, 710–712.
5 S. Inagaki, Y. Fukushima and K. Kuroda, *J. Chem. Soc., Chem. Commun.*, 1993, 680–682.
6 S. Inagaki, S. Guan, Y. Fukushima, T. Ohsuna and O. Terasaki, *J. Am. Chem. Soc.*, 1999, **121**, 9611–9614.
7 B. J. Melde, B. T. Holland, C. F. Blanford and A. Stein, *Chem. Mater.*, 1999, **11**, 3302–3308.
8 T. Asefa, M. J. MacLachlan, N. Coombs and G. A. Ozin, *Nature*, 1999, **402**, 867–871.
9 C. Yoshina-Ishii, T. Asefa, N. Coombs, M. J. MacLachlan and G. A. Ozin, *Chem. Commun.*, 1999, 2539–2540.
10 T. Asefa, C. Yoshina-Ishii, M. J. MacLachlan and G. A. Ozin, *J. Mater. Chem.*, 2000, **10**, 1751–1755.
11 M. J. MacLachlan, T. Asefa and G. A. Ozin, *Chem.–Eur. J.*, 2000, **6**, 2507–2511.
12 A. Stein, B. J. Melde and R. C. Schroden, *Adv. Mater.*, 2000, **12**, 1403–1419.
13 A. Sayari and S. Hamoudi, *Chem. Mater.*, 2001, **13**, 3151–3168.
14 W. J. Hunks and G. A. Ozin, *J. Mater. Chem.*, 2005, **15**, 3716–3724.
15 F. Hoffmann, M. Cornelius, J. Morell and M. Froeba, *Angew. Chem., Int. Ed.*, 2006, **45**, 3216–3251.
16 S. Fujita and S. Inagaki, *Chem. Mater.*, 2008, **20**, 891–908.
17 B. Hatton, K. Landskron, W. Whitnall, D. Perovic and G. A. Ozin, *Acc. Chem. Res.*, 2005, **38**, 305–312.
18 S. Inagaki, S. Guan, T. Ohsuna and O. Terasaki, *Nature*, 2002, **416**, 304–307.
19 M. P. Kapoor, Q. Yang and S. Inagaki, *J. Am. Chem. Soc.*, 2002, **124**, 15176–15177.
20 Y. Lu, H. Fan, N. Doke, D. A. Loy, R. A. Assink, D. A. LaVan and C. J. Brinker, *J. Am. Chem. Soc.*, 2000, **122**, 5258–5261.
21 K. Landskron, B. D. Hatton, D. D. Perovic and G. A. Ozin, *Science*, 2003, **302**, 266–269.
22 A. Fukuoka, Y. Sakamoto, S. Guan, S. Inagaki, N. Sugimoto, Y. Fukushima, K. Hirahara, S. Iijima and M. Ichikawa, *J. Am. Chem. Soc.*, 2001, **123**, 3373–3374.
23 M. P. Kapoor, A. Bhaumik, S. Inagaki, K. Kuraoka and T. Yazawa, *J. Mater. Chem.*, 2002, **12**, 3078–3083.
24 A. Bhaumik, M. P. Kapoor and S. Inagaki, *Chem. Commun.*, 2003, 470–471.
25 S. Shylesh and A. P. Singh, *Microporous Mesoporous Mater.*, 2006, **94**, 127–138.
26 M. C. Burleigh, S. Dai, E. W. Hagaman and J. S. Lin, *Chem. Mater.*, 2001, **13**, 2537–2546.
27 M. C. Burleigh, M. A. Markowitz, M. S. Spector and B. P. Gaber, *Environ. Sci. Technol.*, 2002, **36**, 2515–2518.
28 S. Hudson, J. Cooney, B. K. Hodnett and E. Magner, *Chem. Mater.*, 2007, **19**, 2049–2055.
29 C. Li, J. Liu, X. Shi, J. Yang and Q. Yang, *J. Phys. Chem. C*, 2007, **111**, 10948–10954.
30 T. Asefa, M. J. MacLachlan, H. Grondey, N. Coombs and G. A. Ozin, *Angew. Chem., Int. Ed.*, 2000, **39**, 1808–1811.
31 S. Guan, S. Inagaki, T. Ohsuna and O. Terasaki, *J. Am. Chem. Soc.*, 2000, **122**, 5660–5661.
32 A. Ide, R. Voss, G. Scholz, G. A. Ozin, M. Antonietti and A. Thomas, *Chem. Mater.*, 2007, **19**, 2649–2657.
33 L. Gao, F. Wei, Y. Zhou, X. X. Fan, Y. Wang and J. H. Zhu, *Chem.–Eur. J.*, 2009, **15**, 8310–8318.
34 M. Kuroki, T. Asefa, W. Whitnal, M. Kruk, C. Yoshina-Ishii, M. Jaroniec and G. A. Ozin, *J. Am. Chem. Soc.*, 2002, **124**, 13886–13895.
35 K. Landskron and G. A. Ozin, *Angew. Chem., Int. Ed.*, 2005, **44**, 2107–2109.
36 W.-H. Zhang, X. Zhang, Z. Hua, P. Harish, F. Schroeder, S. Hermes, T. Cadenbach, J. Shi and R. A. Fischer, *Chem. Mater.*, 2007, **19**, 2663–2670.
37 L. Zhang, H. C. L. Abbenhuis, Q. Yang, Y.-M. Wang, P. C. M. M. Magusin, B. Mezari, R. A. van Santen and C. Li, *Angew. Chem., Int. Ed.*, 2007, **46**, 5003–5006.
38 W. J. Hunks and G. A. Ozin, *Adv. Funct. Mater.*, 2005, **15**, 259–266.
39 K. Landskron and G. A. Ozin, *Science*, 2004, **306**, 1529–1532.
40 M. C. Burleigh, S. Jayasundera, M. S. Spector, C. W. Thomas, M. A. Markowitz and B. P. Gaber, *Chem. Mater.*, 2003, **16**, 3–5.
41 T. Asefa, M. Kruk, M. J. MacLachlan, N. Coombs, H. Grondey, M. Jaroniec and G. A. Ozin, *J. Am. Chem. Soc.*, 2001, **123**, 8520–8530.
42 M. C. Burleigh, M. A. Markowitz, M. S. Spector and B. P. Gaber, *J. Phys. Chem. B*, 2001, **105**, 9935–9942.
43 R. M. Grudzien, B. E. Grabicka, S. Pikus and M. Jaroniec, *Chem. Mater.*, 2006, **18**, 1722–1725.
44 M. Alvaro, B. Ferrer, V. Fornes and H. Garcia, *Chem. Commun.*, 2001, 2546–2547.
45 M. Alvaro, B. Ferrer, H. Garcia and F. Rey, *Chem. Commun.*, 2002, 2012–2013.
46 O. Olkhovyk and M. Jaroniec, *J. Am. Chem. Soc.*, 2005, **127**, 60–61.
47 E.-B. Cho, D. Kim, J. Gorka and M. Jaroniec, *J. Phys. Chem. C*, 2009, **113**, 5111–5119.
48 W. Guo, I. Kim and C.-S. Ha, *Chem. Commun.*, 2003, 2692–2693.
49 L. Zhao, G. Zhu, D. Zhang, Y. Di, Y. Chen, O. Terasaki and S. Qiu, *J. Phys. Chem. B*, 2005, **109**, 764–768.

50 Y. Liang, M. Hanzlik and R. Anwander, *Chem. Commun.*, 2005, 525–527.
51 Z. Zhang, X. Yan, B. Tian, S. Shen, D. Chen, G. Zhu, S. Qiu and D. Zhao, *Chem. Lett.*, 2005, **34**, 182–183.
52 H. I. Lee, C. Pak, S. H. Yi, J. K. Shon, S. S. Kim, B. G. So, H. Chang, J. E. Yie, Y.-U. Kwon and J. M. Kim, *J. Mater. Chem.*, 2005, **15**, 4711–4717.
53 Y. Liang, M. Hanzlik and R. Anwander, *J. Mater. Chem.*, 2006, **16**, 1238–1253.
54 D. Zhao, Q. Huo, J. Feng, B. F. Chmelka and G. D. Stucky, *J. Am. Chem. Soc.*, 1998, **120**, 6024–6036.
55 F. Kleitz, S. H. Choi and R. Ryoo, *Chem. Commun.*, 2003, 2136–2137.
56 J. R. Matos, M. Kruk, L. P. Mercuri, M. Jaroniec, L. Zhao, T. Kamiyama, O. Terasaki, T. J. Pinnavaia and Y. Liu, *J. Am. Chem. Soc.*, 2003, **125**, 821–829.
57 T. W. Kim, R. Ryoo, M. Kruk, K. P. Gierszal, M. Jaroniec, S. Kamiya and O. Terasaki, *J. Phys. Chem. B*, 2004, **108**, 11480–11489.
58 J. Fan, C. Yu, J. Lei, Q. Zhang, T. Li, B. Tu, W. Zhou and D. Zhao, *J. Am. Chem. Soc.*, 2005, **127**, 10794–10795.
59 L. Cao, T. Man and M. Kruk, *Chem. Mater.*, 2009, **21**, 1144–1153.
60 S. Hamoudi, Y. Yang, I. L. Moudrakovski, S. Lang and A. Sayari, *J. Phys. Chem. B*, 2001, **105**, 9118–9123.
61 V. Rebbin, M. Jakubowski, S. Pötz and M. Fröba, *Microporous Mesoporous Mater.*, 2004, **72**, 99–104.
62 N. Bion, P. Ferreira, A. Valente, I. S. Goncalves and J. Rocha, *J. Mater. Chem.*, 2003, **13**, 1910–1913.
63 S. S. Park and C.-S. Ha, *Chem. Mater.*, 2005, **17**, 3519–3523.
64 M. C. Burleigh, M. A. Markowitz, M. S. Spector and B. P. Gaber, *J. Phys. Chem. B*, 2002, **106**, 9712–9716.
65 O. Muth, C. Schellbach and M. Froeba, *Chem. Commun.*, 2001, 2032–2033.
66 H. Zhu, D. J. Jones, J. Zajac, J. Roziere and R. Dutartre, *Chem. Commun.*, 2001, 2568–2569.
67 J. R. Matos, M. Kruk, L. P. Mercuri, M. Jaroniec, T. Asefa, N. Coombs, G. A. Ozin, T. Kamiyama and O. Terasaki, *Chem. Mater.*, 2002, **14**, 1903–1905.
68 W.-H. Zhang, B. Daly, J. O'Callaghan, L. Zhang, J.-L. Shi, C. Li, M. A. Morris and J. D. Holmes, *Chem. Mater.*, 2005, **17**, 6407–6415.
69 X. Y. Bao, X. Li and X. S. Zhao, *J. Phys. Chem. B*, 2006, **110**, 2656–2661.
70 W. Guo, J.-Y. Park, M.-O. Oh, H.-W. Jeong, W.-J. Cho, I. Kim and C.-S. Ha, *Chem. Mater.*, 2003, **15**, 2295–2298.
71 X. Y. Bao, X. S. Zhao, X. Li, P. A. Chia and J. Li, *J. Phys. Chem. B*, 2004, **108**, 4684–4689.
72 X. Bao, X. S. Zhao, X. Li and J. Li, *Appl. Surf. Sci.*, 2004, **237**, 380–386.
73 E.-B. Cho and K. Char, *Chem. Mater.*, 2004, **16**, 270–275.
74 W. Wang, S. Xie, W. Zhou and A. Sayari, *Chem. Mater.*, 2004, **16**, 1756–1762.
75 C. Vercaemst, H. Friedrich, P. E. de Jongh, A. V. Neimark, B. Goderis, F. Verpoort and P. Van Der Voort, *J. Phys. Chem. C*, 2009, **113**, 5556–5562.
76 Y. Goto and S. Inagaki, *Chem. Commun.*, 2002, 2410–2411.
77 J. Morell, G. Wolter and M. Froba, *Chem. Mater.*, 2005, **17**, 804–808.
78 A. Kuschel, H. Sievers and S. Polarz, *Angew. Chem., Int. Ed.*, 2008, **47**, 9513–9517.
79 Y.-T. Chan, H.-P. Lin, C.-Y. Mou and S.-T. Liu, *Microporous Mesoporous Mater.*, 2009, **123**, 331–337.
80 R. Ryoo, I.-S. Park, S. Jun, C. W. Lee, M. Kruk and M. Jaroniec, *J. Am. Chem. Soc.*, 2001, **123**, 1650–1657.
81 Y. Deng, T. Yu, Y. Wan, S. Shi, Y. Meng, D. Gu, L. Zhang, Y. Huang, C. Liu, X. Wu and D. Zhao, *J. Am. Chem. Soc.*, 2007, **129**, 1690–1697.
82 M. C. Burleigh, M. A. Markowitz, E. M. Wong, J.-S. Lin and B. P. Gaber, *Chem. Mater.*, 2001, **13**, 4411–4412.
83 Y. Liang and R. Anwander, *Microporous Mesoporous Mater.*, 2004, **72**, 153–165.
84 D. Jiang, J. Gao, J. Li, Q. Yang and C. Li, *Microporous Mesoporous Mater.*, 2008, **113**, 385–392.
85 K. Nakanishi and K. Kanamori, *J. Mater. Chem.*, 2005, **15**, 3776–3786.
86 C. Vercaemst, P. E. de Jongh, J. D. Meeldijk, B. Goderis, F. Verpoort and P. Van Der Voort, *Chem. Commun.*, 2009, 4052–4054.
87 X. Zhou, S. Qiao, N. Hao, X. Wang, C. Yu, L. Wang, D. Zhao and G. Q. Lu, *Chem. Mater.*, 2007, **19**, 1870–1876.
88 J.-S. Chung, D.-J. Kim, W.-S. Ahn, J.-H. Ko and W.-J. Cheong, *Korean J. Chem. Eng.*, 2004, **21**, 132–139.
89 H. Zhong, G. Zhu, J. Yang, P. Wang and Q. Yang, *Microporous Mesoporous Mater.*, 2007, **100**, 259–267.
90 H. Zhang, J. Sun, D. Ma, G. Weinberg, D. S. Su and X. Bao, *J. Phys. Chem. B*, 2006, **110**, 25908–25915.
91 J. Sun, H. Zhang, D. Ma, Y. Chen, X. Bao, A. Klein-Hoffmann, N. Pfaender and D. S. Su, *Chem. Commun.*, 2005, 5343–5345.
92 M. Kruk and L. Cao, *Langmuir*, 2007, **23**, 7247–7254.
93 M. Kruk and C. M. Hui, *Microporous Mesoporous Mater.*, 2008, **114**, 64–73.
94 P. Schmidt-Winkel, W. W. Lukens, Jr, D. Zhao, P. Yang, B. F. Chmelka and G. D. Stucky, *J. Am. Chem. Soc.*, 1999, **121**, 254–255.
95 A. Sayari, M. Kruk, M. Jaroniec and I. L. Moudrakovski, *Adv. Mater.*, 1998, **10**, 1376–1379.
96 R. Nagarajan, *Colloids Surf., B*, 1999, **16**, 55–72.
97 R. Nagarajan, M. Barry and E. Ruckenstein, *Langmuir*, 1986, **2**, 210–215.
98 D. Zhao, J. Feng, Q. Huo, N. Melosh, G. H. Frederickson, B. F. Chmelka and G. D. Stucky, *Science*, 1998, **279**, 548–552.
99 J. Rouquerol, D. Avnir, C. W. Fairbridge, D. H. Everett, J. H. Haynes, N. Pernicone, J. D. F. Ramsay, K. S. W. Sing and K. K. Unger, *Pure Appl. Chem.*, 1994, **66**, 1739–1758.
100 E. P. Barrett, L. G. Joyner and P. P. Halenda, *J. Am. Chem. Soc.*, 1951, **73**, 373–380.
101 M. Kruk, M. Jaroniec and A. Sayari, *Langmuir*, 1997, **13**, 6267–6273.
102 M. Jaroniec, M. Kruk and J. P. Olivier, *Langmuir*, 1999, **15**, 5410–5413.
103 L. Cao and M. Kruk, *Colloids Surf., A*, 2010, **357**, 91–96.
104 M. Kruk and M. Jaroniec, *Chem. Mater.*, 2003, **15**, 2942–2949.
105 P. Van Der Voort, P. I. Ravikovitch, K. P. De Jong, M. Benjelloun, E. Van Bavel, A. H. Janssen, A. V. Neimark, B. M. Weckhuysen and E. F. Vansant, *J. Phys. Chem. B*, 2002, **106**, 5873–5877.
106 M. Kruk, M. Jaroniec, S. H. Joo and R. Ryoo, *J. Phys. Chem. B*, 2003, **107**, 2205–2213.
107 R. Ryoo, C. H. Ko, M. Kruk, V. Antochshuk and M. Jaroniec, *J. Phys. Chem. B*, 2000, **104**, 11465–11471.
108 M. P. Kapoor, S. Inagaki, S. Ikeda, K. Kakiuchi, M. Suda and T. Shimada, *J. Am. Chem. Soc.*, 2005, **127**, 8174–8178.

